Fidgetin interacting with microtubule end binding protein EB3 affects axonal regrowth in spinal cord injury

Chao Ma[1, 2], Junpei Wang[1], Qifeng Tu[1], Weijuan Bo[1], Zunlu Hu[1], Run Zhuo[1], Ronghua Wu[1], Zhangji Dong[1], Liang Qiang[3], Yan Liu[1], Mei Liu[1, *]

https://doi.org/10.4103/1673-5374.373716

Date of submission: November 8, 2022

Date of decision: January 30, 2023

Date of acceptance: March 11, 2023

Date of web publication: April 20, 2023

From the Contents

Graphical Abstract

Fidgetin interacting with EB3 affects axonal regrowth and branching

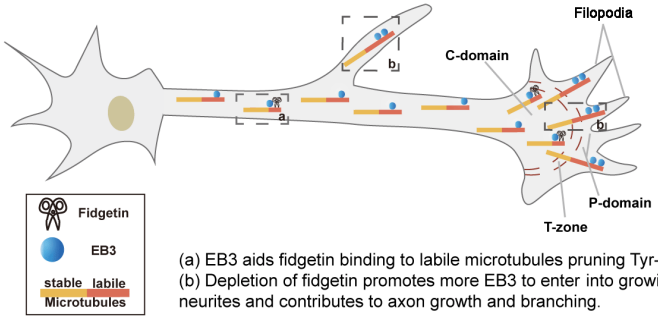

(a) EB3 aids fidgetin binding to labile microtubules pruning Tyr-tubulin. (b) Depletion of fidgetin promotes more EB3 to enter into growing neurites and contributes to axon growth and branching.

Abstract

Fidgetin, a microtubule-severing enzyme, regulates neurite outgrowth, axonal regeneration, and cell migration by trimming off the labile domain of microtubule polymers. Because maintenance of the microtubule labile domain is essential for axon initiation, elongation, and navigation, it is of interest to determine whether augmenting the microtubule labile domain via depletion of fidgetin serves as a therapeutic approach to promote axonal regrowth in spinal cord injury. In this study, we constructed rat models of spinal cord injury and sciatic nerve injury. Compared with spinal cord injury, we found that expression level of tyrosinated microtubules in the labile portion of microtubules continuously increased, whereas fidgetin decreased after peripheral nerve injury. Depletion of fidgetin enhanced axon regeneration after spinal cord injury, whereas expression level of end binding protein 3 (EB3) markedly increased. Next, we performed RNA interference to knockdown EB3 or fidgetin. We found that deletion of EB3 did not change fidgetin expression. Conversely, deletion of fidgetin markedly increased expression of tyrosinated microtubules and EB3. Deletion of fidgetin increased the amount of EB3 at the end of neurites and thereby increased the level of tyrosinated microtubules. Finally, we deleted EB3 and overexpressed fidgetin. We found that fidgetin trimmed tyrosinated tubulins by interacting with EB3. When fidgetin was deleted, the labile portion of microtubules was elongated, and as a result the length of axons and number of axon branches were increased. These findings suggest that fidgetin can be used as a novel therapeutic target to promote axonal regeneration after spinal cord injury. Furthermore, they reveal an innovative mechanism by which fidgetin preferentially severs labile microtubules.

Key Words: acetylated microtubules; axon regeneration; axonal branching; axonal regrowth; end binding protein 3; fidgetin; microtubule dynamics; sciatic nerve injury; spinal cord injury; tyrosinated microtubules

Introduction

Axons do not easily regenerate following adult mammalian spinal cord injury (SCI), and therefore improving axonal regenerative capacity after injury remains highly relevant in neuroscience. The manipulation of cytoskeletal dynamics through different approaches has been suggested as an effective strategy to promote neural repair (Blanquie and Bradke, 2018; Xu et al., 2021; Min et al., 2022). Damaged microtubules (MTs) form a non-regenerative retracted bulb at the distal end of the axon, which prohibits axonal regeneration after SCI (Hur et al., 2012; Sofroniew, 2018). Most patients with SCI retain residual axons (Fawcett et al., 2007; Lasiene et al., 2008), but the injured axons are unable to regenerate, possibly because of disrupted MT dynamicity (Kulkarni et al., 2022). Thus, strategies to increase MT dynamicity for promoting axonal regrowth are of great interest in developing innovative approaches to treat neural injuries (Anderson et al., 2018).

MT dynamics is required for the homeostasis of neuronal functions such as growth cone pathfinding, axon outgrowth and branching, as well as axonal transport of vesicles and organelles (Liu et al., 2022). Detyrosination/tyrosination is a reversible tubulin post-translational modification that contributes to various cellular processes, particularly in the nervous system (Fukushima et al., 2009; Song and Brady, 2015). Studies suggest that tyrosinated (Tyr)-tubulin is discontinuously distributed along the axon, being abundant in the axon initial segment, distal axon, and growth cone, but of relatively low abundance in the axonal shaft (Baas and Black, 1990). This pattern indicates that Tyr-tubulin might participate in controlling cargo movement in and out of the axon initial segment (Nirschl et al., 2016) and modulating growth cone navigation in the distal axon.

Neurons express abundant MT-severing proteins as they play essential roles in various cellular functions and behaviors. So far, three major MT-severing proteins have been identified in neurons: spastin, katanin, and fidgetin (Fign), all of which belong to the ATPases protein family, which in turn is associated with diverse cellular activities (McNally and Roll-Mecak, 2018). Among these three ATPases, katanin and spastin have been extensively investigated. Lines of evidence indicate that both katanin and spastin perform potent MT severing activities, which contribute to fueling more short MTs into axons. This substantially affects axon outgrowth, branching, and navigation (Ahmad et al., 1999; Yu et al., 2008; Vemu et al., 2018). Interestingly, katanin and spastin appear to possess a severing propensity towards the stable domain of MTs instead of the labile domain (Ji et al., 2018; Shin et al., 2019). Moreover, various binding partners for each MT-severing protein have

[1]Key Laboratory of Neuroregeneration of Jiangsu and Ministry of Education, Co-innovation Center of Neuroregeneration, NMPA Key Laboratory for Research and Evaluation of Tissue Engineering Technology Products, Nantong University, Nantong, Jiangsu Province, China; [2]Medical School of Nantong University, Nantong, Jiangsu Province, China; [3]Department of Neurobiology and Anatomy, Drexel University College of Medicine, Philadelphia, PA, USA

*Correspondence to: Mei Liu, PhD, liumei@ntu.edu.cn.

https://orcid.org/0000-0003-1168-6119 (Mei Liu)

Funding: *This study was supported by the National Natural Science Foundation of China, Nos. 32070725 (to ML), 82001295 (to RHW), 31970412 (to YL); and the Priority Academic Program Development (PAPD) of Jiangsu Higher Education Institutions.*

How to cite this article: *Ma C, Wang J, Tu Q, Bo W, Hu Z, Zhuo R, Wu R, Dong Z, Qiang L, Liu Y, Liu M (2023) Fidgetin interacting with microtubule end binding protein EB3 affects axonal regrowth in spinal cord injury. Neural Regen Res 18(12):2727-2732.*

been uncovered, providing a potential mechanistic basis for their activities. However, until recently, limited work has been performed on the functional activities of Fign in neurons. Fign was initially identified as a key protein whose absence leads to significant developmental defects in mice (Cox et al., 2000). The MT severing activity of Fign was confirmed in previous studies (Mukherjee et al., 2012; Tao et al., 2016). Only recently, Fign was shown to be involved in axon growth and branching with a striking preference towards severance of the labile domain of axonal MTs (which is opposite to katanin and spastin) (Leo et al., 2015; Austin et al., 2017; Matamoros et al., 2019). Unlike katanin and spastin, whose overexpression leads to visible short MT fragments, Fign overexpression does not appear to have such an effect (Roll-Mecak and McNally, 2010; Hu et al., 2017; Vemu et al., 2018). In addition, we previously found that Fign depletion by small interfering RNA (siRNA) substantially increased Tyr-MTs in astrocytes (Hu et al., 2017). Interestingly, Fign knockdown in cultured dorsal root ganglion (DRG) neurons increased axon length and promoted axon regeneration after DRG injury *in vivo* owing to augmentation of labile MTs (Leo et al., 2015; Austin et al., 2017; Matamoros et al., 2019). So far, it is unclear how Fign preferentially targets labile MTs in axons.

In this study, we compared the expression of Tyr-MTs after SCI and peripheral nerve injury. Furthermore, we determined whether alteration of Tyr-MTs facilitate axon regeneration after SCI, and accordingly, whether Fign could serve as a putative therapeutic target. More importantly, we sought to identify a mechanistic pathway that underlies its propensity towards the labile MT domain.

Methods

Model establishment of SCI and sciatic nerve injury

In total, 36 adult male Sprague-Dawley rats (specific pathogen-free level, aged 8-week-old, weight 200–240 g) were provided by the Laboratory Animal Center of Nantong University (Nantong, China; license No. SYXK (Su) 2020-0029). The rats were housed at 24°C and 55 ± 5% humidity with a 12-hour light/dark cycle. All animal surgeries were conducted in accordance with Institutional Animal Care guidelines, as well as with National Institutes of Health guidelines (Bethesda, MD, USA) (NIH publication No. 85-23, 1985, revised 1996). This study was approved by the Animal Ethics Committee of Nantong University, China (document No. S20200330-005) on March 30, 2020.

Spinal cord contusion

The rats were randomly divided into six groups (0-, 3-, 7-, 14-, 21- and 28-day groups), each of which included three rats. Briefly, all animals were anesthetized with oxygenated air and isoflurane (concentration of anesthesia induction was 2.5% and exposure time was 5 minutes, concentration of maintenance was 2%; provided by RWD Life Science, Shenzhen, Guangdong, China), which was administered by an anesthesia machine (RWD Life Science). To fully expose the spinal cord, a laminectomy at the T10 vertebrae was performed followed by a layer-by-layer incision through the skin, subcutaneous tissues, and fascia to separate the lateral muscle tissues. Afterwards, the exposed spinal cord segment (about 5 mm in length) received a 160 kilodyne spinal contusion injury, which was applied for 30 seconds for each rat using an Impactor injury device (Pressure Systems International, San Antonio, TX, USA). To prevent infection, 100 µL gentamicin (Quanyu Life Science, Shanghai, China) was applied at the surgical site. Postoperative treatments included injection of penicillin solution for the first 7 days and manual bladder emptying twice a day as in our previous study (Wu et al., 2019). Subsequently, the rats were sacrificed and a total of 1 cm spinal samples above and below the site of injury was harvested on days 3, 7, 14, 21, and 28 after treatment.

Sciatic nerve crush

Other rats were randomly divided into six groups (0-, 3-, 7-, 14-, 21- and 28-day groups), each of which included three rats. As described in our previous study (Wu et al., 2015), rats were anesthetized and the right lateral sciatic nerve was exposed through an incision made mid-thigh on the lateral side of the hind leg. The nerve was crushed three times using a microsurgical hemostatic forceps to the third button for 10 seconds each time at 10-second intervals. To prevent infection, 100 µL gentamicin-saline was applied at the surgical site. Subsequently, the rats were sacrificed and sciatic nerve samples (including L4–L6 DRG ganglia) were harvested on days 3, 7, 14, 21, and 28 after treatment.

Functional behavioral evaluation

The Basso-Beattie-Bresnahan (BBB) locomotion scale (Basso et al., 1995) was used to evaluate the motor capacity of rats on days 1, 4, 7, 10, and 14 post-SCI. Detailed methods are published in our previous study (Ma et al., 2023).

AAV9-U6-shRNA-GFP infection

For knockdown of Fign, adeno-associated viruses (AAV) serotype 9 for U6-shFign-green fluorescent protein (GFP) and control shRNA-GFP were customized by Genechem (Shanghai, China). Overall, 30 rats were randomly divided into control shRNA and Fign shRNA groups, each of which included fifteen rats. As described previously (Ma et al., 2023), rats were injected with 2.7 µL of AAV-shFign using a glass micropipette (tip diameter ~20 µm) attached to a Nanoliter 2000 pressure injection apparatus (World Precision Instruments, Sarasota, FL, USA). Two weeks before modeling (spinal cord contusion), a total of 2.7 µL virus was injected at all three T8 sites; each site had three different depths (0.9, 1.2, and 1.5 mm; 300 nL/depth) (virus titer: 5×10^{12} TU/mL).

siRNA treatment and gene overexpression

All siRNAs were synthesized by GenePharma (Suzhou, China). The siRNA was electroporated into cells using an electroscope at 275 V for 0.8 ms (NEPA GENE, Chiba, Japan), in accordance with the manufacturer's instructions. The efficiency of siRNA transfection was confirmed by quantitative polymerase chain reaction (qPCR) and western blotting. To permit protein depletion, the cells were collected after culture for 3 days. The sequences of qPCR primers and end binding protein 3 (EB3) siRNA, Fign siRNA, and Ctrl siRNA are listed in **Table 1**.

Table 1 | **The sequences for siRNA, and primers in quantitative polymerase chain reaction**

Name	Sequence (5'–3')
Ctrl siRNA	Sense: UUC UCC GAA CGU GUC ACG UTT
	Antisense: ACG UGA CAC GUU CGG AGA ATT
Fign siRNA	Sense: GGA UCG UAU UUG CAU UCU ATT
	Antisense: UAG AAU GCA AAU ACG AUC CTT
EB3 siRNA	Sense: GCC GUC AAU GUG UAC UCC ATT
	Antisense: UGG AGU ACA CAU UGA CGG CTT
Fign	Sense: TTT GTG CCA CCA GTA AAC CA
	Antisense: ACG AGC AGT GCA AAC TCC TT
GAPDH	Sense: CCA TCA CTG CCA CTC AGA AGA CT
	Antisense: ACA TTG GGG GTA GGA ACA CG

EB3: End binding protein 3; Fign: fidgetin; GAPDH: glyceraldehyde-3-phosphate dehydrogenase; siRNA: small interfering RNA.

The lentivirus (LV)5-Fign, which was used in our previous study (Hu et al., 2017), was purchased from GenePharma and applied to cultured neurons at a multiplicity of infection = 40 TU/cell. For 24-well plates, 1×10^5 cells were transfected with Ctrl siRNA or EB3 siRNA before plating, then neurons were cultured for 6 hours before addition of the virus. Fresh medium was provided after 18 hours of incubation and neurons were fixed to perform immunostaining after LV5-Fign overexpression for 3 days.

Cell culture

Cortical neurons

Cortical neurons from rat embryos at 18 days (E18) were collected from six pregnant Sprague-Dawley rats (specific pathogen-free level) were provided by the Laboratory Animal Center of Nantong University). E18 neurons were isolated, purified, and cultured according to our previous studies (Qiang et al., 2018; Ma et al., 2021; Teng et al., 2021). The cells were cultured in Neurobasal medium (Thermo Fisher, Waltham, MA, USA) supplemented with 2% NeuroCult SM1 Neuronal Supplement (Stem Cell, Vancouver, BC, Canada), 0.5 mM glutamine (Beyotime, Shanghai, China), and 1% penicillin-streptomycin (Beyotime). Neuronal cultures were considered appropriate for use when they were 95% positive for Tuj1.

Astrocytes

Primary astrocytes were obtained and cultured according to our previous studies (Feng et al., 2016; Hu et al., 2017). Briefly, 20 Sprague-Dawley rat pups (postnatal day 1) were obtained from the Laboratory Animal Center of Nantong University and were anesthetized with isoflurane as above. Brains were dissected, digested, and then gently passed through a sterile 75-µm Nitex mesh. The cell suspension was plated into culture flasks. When astrocytes became confluent, the cultures were shaken at 150 r/min for 16 hours to purify the cultures. The cells were cultured in Dulbecco's modified Eagle medium (DMEM)/F-12 (Invitrogen, Waltham, MA, USA) supplemented with 10% fetal bovine serum, 0.5 mM glutamine, and 1% penicillin-streptomycin. Astrocyte cultures were considered appropriate for use when they were 95% positive for glial fibrillary acidic protein.

Neuro-2a cells

The Neuro-2a cell line, TCM29 (Cell Bank of Chinese Academy of Sciences, Shanghai, China; RRID: CVCL_0470) was commercially available from the Shanghai Cell Bank of the Chinese Academy of Sciences. According to the manufacturer's instructions, cells were cultured in DMEM supplemented with 10% fetal bovine serum, 0.5 mM glutamine, and 1% penicillin-streptomycin. All cells were incubated in a humidified atmosphere of 95% air and 5% CO_2 at 37°C.

qRT-PCR

Total RNA was extracted from cultured neurons using a RaPure Total RNA Micro kit (Magen, Shanghai, China). RNA was then reverse-transcribed using HiScriptII 1st Strand cDNA Synthesis Kit (Vazyme, Nanjing, China) and amplified using a qPCR system (Applied Biosystems, Waltham, MA, USA) with AceQ qPCR SYBR Green Master mix (High ROX Premixed; Vazyme, Nanjing, China). The primer sequences used to amplify Fign and glyceraldehyde-3-phosphate dehydrogenase (GAPDH) are shown in **Table 1** with 95°C per-incubation for 5 minutes and 40 cycles with 95°C 10 seconds, 60°C 10 seconds and 72°C 40 seconds. The results were calculated by $2^{-\Delta\Delta CT}$ method (Cao et al., 2022).

Western blotting

For western blotting, cells (cultured neurons or astrocytes) or tissues (spinal cord or sciatic nerve) were lysed for extraction of total protein. Protein samples were separated using sodium dodecyl sulfate-polyacrylamide gel electrophoresis. After transfer to a polyvinylidene fluoride membrane (Millipore, Boston, MA, USA), the membrane was blocked and then incubated overnight with primary antibodies at 4°C: anti-α/β tubulin (rabbit, 1:2000, CST, Danvers, MA, USA, Cat# 2148, RRID: AB_2288042), anti-tyrosinated tubulin (rat, 1:800, Abcam, Cambridge, UK, Cat# ab6160, RRID: AB_305328), anti-acetylated tubulin (mouse, 1:800, Abcam, Cat# ab24610, RRID: AB_448182), anti-Fign (mouse, 1:400, Santa Cruz Biotechnology, Santa Cruz, CA, USA, Cat# sc-514956), anti-GFP (rabbit, 1:1000, CST, Cat# 2555, RRID: AB_10692764), and anti-EB3 (rabbit, 1:20,000, Abcam, Cat# ab157217, RRID: AB_2890656). Next, horseradish peroxidase-conjugated secondary antibodies (both 1:2000, anti-mouse, Cat# A0216, RRID: AB_2860575, or anti-rabbit, Cat# A0208, RRID: AB_2892644; Beyotime) were applied at 20–24°C for 2 hours after washing with Tris-buffered saline with 0.1% Tween 20. Immunoreactive bands were visualized using ECL chemiluminescence kit (Tanon, Shanghai China). The optical density was analyzed using ImageJ software (version 1.53t, National Institutes of Health) (Schneider et al., 2012).

Fluorescence staining

Immunostaining was performed according to our previous study (Ma et al., 2023). Briefly, cultured neurons were fixed and extracted with pre-warmed fixation solution (4% paraformaldehyde, 0.2% glutaraldehyde, 2× PHEM [piperazine-1,4-bisethanesulfonic acid + 2-[4-(2-hydroxyethyl)-1-piperazinyl] ethanesulfonic acid + ethylenebis(oxyethylenenitrilo)tetraacetic acid + $MgCl_2$], and 0.1% Triton X-100) for 20 minutes. Cultured astrocytes and Neuro-2a cells were fixed with pre-warmed 4% paraformaldehyde. Fresh spinal cord tissue slides were post-fixed in 4% paraformaldehyde for 16 hours, dehydrated through a series of sucrose solutions, and then embedded with optimal cutting temperature compound. Cells or slices were washed three-times with phosphate-buffered saline (PBS) and blocked with 10% normal goat serum at 37°C for 30 minutes or 2 hours. Primary antibodies were as follows: anti-α-tubulin (rabbit, 1:1200, Abcam, Cat# ab18251, RRID: AB_2210057), anti-tyrosinated tubulin (rat, 1:800, Abcam, Cat# ab6160, RRID: AB_305328), anti-acetylated tubulin (mouse, 1:500, Abcam, Cat# ab24610, RRID: AB_448182), anti-Tuj1 (mouse, 1:800, Biolegend, San Diego, CA, USA, Cat# 801201, RRID: AB_2313773), anti-Fign (rabbit, 1:200, Abcam, Cat# ab232756), anti-EB3 (rabbit, 1:500, Abcam, Cat# ab157217, RRID: AB_2890656), anti-EB3 (rat, 1:450, Santa Cruz Biotechnology, Cat# sc-101475, RRID: AB_2141771), anti-actin (mouse, 1:1000, Proteintech, Rosemont, IL, USA, Cat# 60008-1-Ig, RRID: AB_2289225), and anti-neurofilament-200 (NF200) (rabbit, 1:200, Sigma, Cat# N4142, RRID: AB_477272). Primary antibodies were incubated at 4°C overnight. Next, corresponding secondary antibodies were applied at 20–24°C for 2 hours (Alexa Flour 488-conjugated AffiniPure Goat Anti-Mouse IgG(H+L), 1:800, Jackson ImmunoResearch Laboratories, West Grove, PA, USA, Cat# 115-545-003, RRID: AB_2338840; Alexa Flour 488-conjugated AffiniPure Goat Anti-Rabbit IgG(H+L), 1:800, Jackson ImmunoResearch Laboratories, Cat# 111-545-003, RRID:AB_2338046; Alexa Flour Cy3-conjugated AffiniPure Goat Anti-Mouse IgG(H+L), 1:800, Jackson ImmunoResearch Laboratories, Cat# 115-165-003, RRID: AB_2338680; Alexa Flour Cy3-conjugated AffiniPure Goat Anti-Rat IgG(H+L), 1:800, Jackson ImmunoResearch Laboratories, Cat# 112-165-003, RRID: AB_2338240; Alexa Flour Cy3-conjugated AffiniPure Goat Anti-Rabbit IgG(H+L), 1:800, Jackson ImmunoResearch Laboratories, Cat# 111-165-003, RRID: AB_2338240; and Alexa Fluor 647 AffiniPure Goat Anti-Rabbit IgG (H+L), 1:800, Jackson ImmunoResearch Laboratories, Cat# 111-605-003, RRID: AB_2338072). Nuclei were stained with Hoechst 33342 (1:2000, Cat# ab228551, Abcam) for 15 minutes. Images were obtained on a Zeiss (Oberkochen, Germany) fluorescence microscope and fluorescence intensity was analyzed by ImageJ.

Co-immunoprecipitation assay

For whole cell lysate co-immunoprecipitation assays, cultured neurons were collected and washed twice with PBS, then lysed in immunoprecipitation lysis buffer for 30 minutes on ice. Antibody was then added (2 μg into 500 μg of total protein) and the reaction incubated overnight at 4°C. For the taxol (paclitaxel) group, taxol (20 nM; MCE, Newark, NJ, USA) was pre-added to the cell culture medium. On day 2, the protein was collected and washed with PBS, and then treated with Pierce® Protein A Agarose (Thermo Fisher) overnight at 4°C. On day 3, co-immunoprecipitation complex-bound resin was collected, and centrifuged for 10 minutes at 2500 × *g*. A 6× loading buffer was added to the complex-bound resin and incubated for 5 minutes at 95°C. The resin mixture was centrifuged at 2500 × *g*, and the supernatant collected and analyzed by western blotting.

Tubulin polymerization assay

Assessment of tubulin polymerization (stability) in cells was performed as described previously (Xu et al., 2018) with modifications. Following Ctrl siRNA or Fign siRNA treatments, Neuro-2a cells were rinsed twice at 37°C with pre-warmed buffer (100 mM piperazine-1,4-bisethanesulfonic acid, pH 6.9, 1 mM $MgCl_2$, 2 mM ethylenebis(oxyethylenenitrilo)tetraacetic acid [PME]), then harvested in PME buffer supplemented with 0.02% Triton X-100 and protease inhibitors. The lysates were centrifuged at 13,000 × *g* for 20 minutes at 20°C. Supernatant (S fraction, protein from supernatant) containing soluble tubulins and the pellet (P fraction, protein from pellet) containing polymerized tubulins were collected separately and analyzed by western blotting.

Statistical analysis

GraphPad Prism 8.0.0 software (GraphPad Software Inc, San Diego, CA, USA) was used for statistical analysis. All experiments were repeated independently at least three times. Data were expressed as mean ± standard error (SE), and all data were tested for normal distribution. Student's *t*-test was used to compare means between two groups, whereas one-way analysis of variance and *post hoc* Dunnett's test was used to compare multiple groups. Two-way analysis of variance and post hoc Bonferroni's test were used to analyze BBB scores. Pearson correlation coefficient was calculated by ImageJ. Values of $P < 0.05$ were considered statistically significant.

Results

Depletion of Fign increases expression of the MT end binding protein, EB3, and enhances functional recovery after SCI

Axonal regeneration is limited in the central nervous system but is available for regeneration in the peripheral nervous system. A previous study reported that after injury of the peripheral nervous system, axonal regeneration was promoted by increasing tubulin dynamics (Cho and Cavalli, 2012). We previously found that Fign knockdown notably increased Tyr-tubulin mass (Hu et al., 2017); therefore, we hypothesized that differences in labile Tyr-MTs (or Tyr-tubulin) may be an important contributing factor. Thus, we established rat models of SCI and sciatic nerve injury, and compared protein alterations in Tyr-tubulin and Fign protein levels by western blotting at 3, 7, 14, 21, and 28 days after injury. Our results show that after SCI (**Figure 1A**) or sciatic nerve injury (**Figure 1B**), Tyr-tubulin increased continuously. The level of Fign decreased slightly after SCI, whereas it was notably decreased after sciatic nerve injury.

These results show that compared with the spinal cord, Tyr-tubulin protein is considerably more abundant in the sciatic nerve. Even after injury, Tyr-tubulin protein showed a rapid increase, which may contribute to peripheral nerve regeneration. In addition, a previous report found that Fign depletion enhanced DRG neuronal regeneration (Matamoros et al., 2019). Thus, we sought to determine whether Tyr-tubulin augmentation due to Fign knockdown contributes to improvement after SCI.

We established the spinal cord contusion model in adult rats as described in our previous study (Zhao et al., 2017). AAV9-U6-shFign was injected to allow Fign depletion (**Figure 1C** and **D**). After injury, we used the BBB score to evaluate behavioral recovery of the rats. Our results show that Fign knockdown improved BBB score, which reached significance on the 14th day post-injury (**Figure 1E**). We also confirmed Fign knockdown efficiency at 14 days post-injury by western blotting (**Figure 1F**). Next, we observed the effects of Fign knockdown by immunohistochemistry at 14 days post-injury. In the Fign-shRNA treated group (**Figure 1G** and **H**), immunopositivity of NF200 was markedly increased in the injured area. These results support our assumption that Fign knockdown improves functional recovery and enhances axonal regeneration after SCI. Interestingly, we found that knockdown of Fign resulted in a significant increase in the MT plus-end binding protein, EB3, which was mostly concentrated in Tyr-tubulin enriched areas (**Figure 1I** and **J**). Our previous study reported that Fign preferentially works on Tyr-tubulin (Hu et al., 2017) and that EB3 usually binds at the growing plus-end of MTs (Qu et al., 2019). These newly added tubulins are tyrosinated. This raises the question of whether Fign is transported to Tyr-MTs via an interaction with EB3.

Knockdown of Fign increases entry of EB3 into growing neurites

Next, we investigated whether Fign depletion affects EB3 expression or localization. First, we confirmed the knockdown efficiency of Fign-siRNA (**Additional Figure 1A** and **B**). We then confirmed that Fign siRNA-treated neurons displayed notably longer axons and more branches than neurons under the control (Ctrl) siRNA treatment (**Additional Figure 1C** and **D**). This phenomenon is consistent with our observation of an increase in NF200 following Fign depletion after SCI. To further examine the relationship between Fign and EB3 expression, we depleted EB3 or Fign using RNA interference and examined changes in their expression. Our results showed that depletion of EB3 did not change expression of Fign (**Figure 2A**). Conversely, depletion of Fign significantly increased expression of EB3 (**Figure 2B**). Depletion of Fign increased the amount of EB3 at the end of neurites (**Figure 2C**). We further analyzed the fluorescence intensity and distribution of EB3 at the distal (15 μm) neurite ends. These results showed that EB3 increased significantly at the distal end of growing neurites after Fign depletion (**Figure 2D**). This suggests that depletion of Fign results in augmentation of the Tyr-tubulin mass by promoting EB3 entry into growing neurites.

Fign conditionally interacts with the MT plus-end binding protein, EB3

Based on the above findings, we next performed endogenous co-immunoprecipitation assays to confirm an interaction between Fign and EB3. Fign antibody pulled-down EB3 protein (**Figure 3A**), whereas EB3 antibody pulled-down Fign when taxol (20 nM) was pre-added to the cell culture medium (**Figure 3B**). Without taxol, the interaction between Fign and EB3 was not detected (**Figure 3C**). This indicates that most Fign is bound to EB3, with only a tiny amount of EB3 bound to Fign. Tyr-MTs are enriched at axonal ends and low doses of taxol leads to EB3 accumulation at the tips of neurites (Witte et al., 2008). Thus, we propose that treatment with a low dose of taxol must increase the chances of EB3 interacting with Fign. Next, we analyzed localization of Fign, EB3, and actin by immunofluorescence staining (**Figure 3D1**). We found co-localization of EB3 and Fign at the axonal shaft and C (central)-domain of growth cones (**Figure 3D2**). Pearson correlation showed

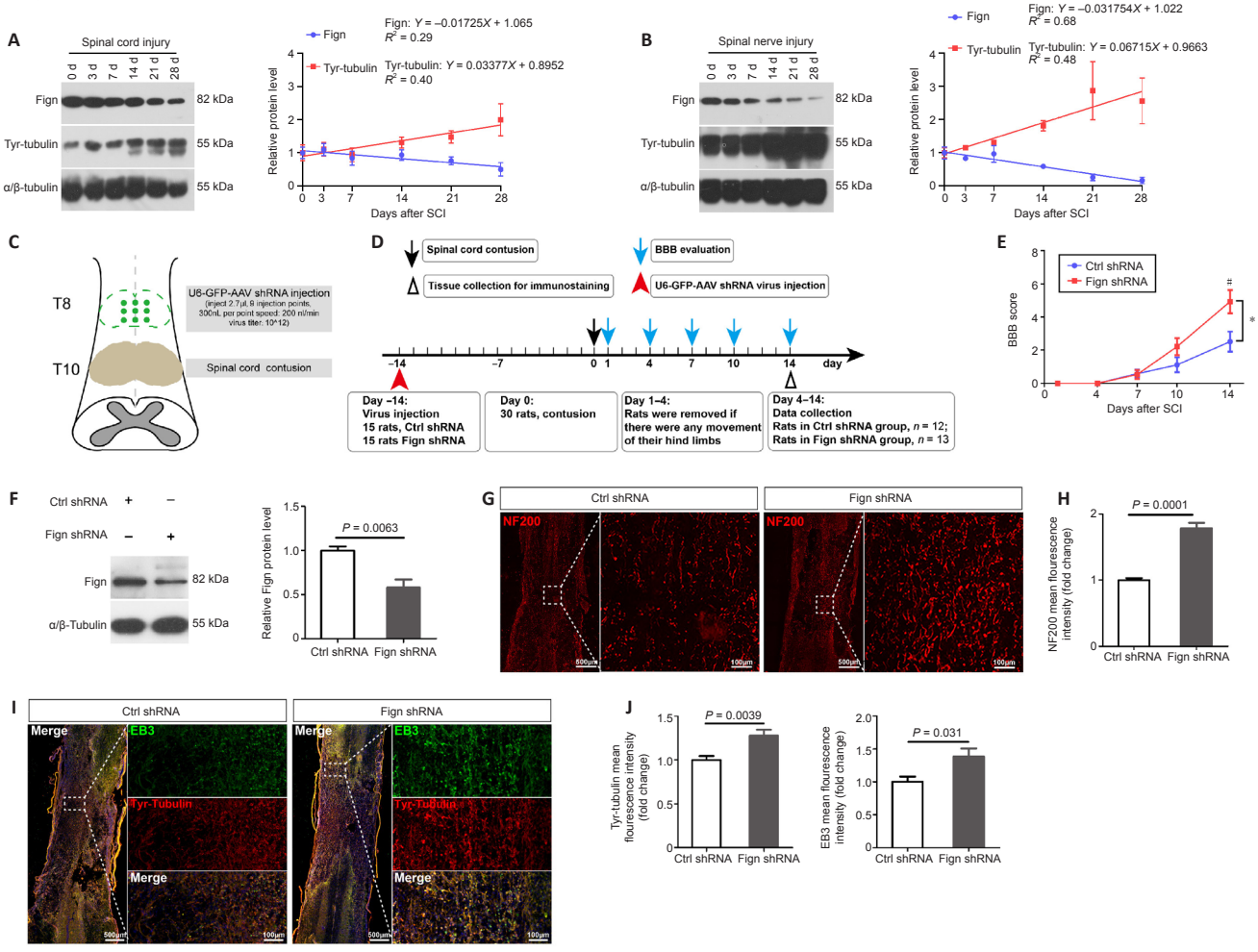

Figure 1 | **Depletion of Fign improves functional recovery by increasing Tyr-tubulin.**
(A, B) Western blotting of tyrosinated (Tyr)-tubulin and Fign after spinal cord contusion (A) and sciatic nerve crush (B). α/β-Tubulin was used as a loading control. The data are shown as mean ± SE (n = 3). The data were normalized by control (0 day) group. Linear regression showed expression trends of target proteins after injury. (C, D) Model of Fign depletion in spinal cord injury: U6-GFP Fign-AAV9 virus injected at T8, spinal cord contusion at T10 (C). Timeline of virus injection, spinal cord contusion, and Basso-Beattie-Bresnahan (BBB) evaluation (D). (E) BBB scores after spinal cord contusion (mean ± SE, n = 12 or 13). *P < 0.05; #P < 0.05, *vs.* Ctrl shRNA group (two-way analysis of variance followed by *post hoc* Bonferroni's test). (F) Representative western blotting of Fign from injured spinal cord at 14 days after spinal cord contusion. α/β-Tubulin was used as a loading control (mean ± SE, n = 4). The data were normalized by Ctrl shRNA group. The data were analyzed by Student's t-test. (G) Representative immunostaining results of NF200 (red, Cy3) in the spinal cord lesion zone at 14 days after spinal cord contusion and treatment with Ctrl or Fign shRNA. Immunopositivity of NF200 was markedly increased in the injured area in the Fign shRNA group. Scale bars: 500 μm, 100 μm (enlarged images). (H) Statistical results of relative NF200 levels (mean ± SE, n = 8, Student's t-test). (I) Representative immunostaining results of Tyr-tubulin and EB3 in the spinal cord lesion zone at 14 days after spinal cord contusion and treatment with Ctrl or Fign shRNA. Microtubule plus-end binding protein EB3 significantly increased and mostly concentrated in Tyr-tubulin enriched areas in the Fign shRNA group. Tyr-tubulin is labeled in red (Alexa Fluor 647) and EB3 in yellow (Cy3) (changed to green by pseudo-color). Scale bars: 500 μm, 100 μm (enlarged images). (J) Statistical results of relative Tyr-tubulin and EB3 levels (mean ± SE, n = 5). The data were normalized by Ctrl shRNA group. The data were analyzed by Student's t-test. AAV: Adeno-associated virus; BBB: Basso-Beattie-Bresnahan; EB3: end binding protein 3; Fign: fidgetin; GFP: green fluorescent protein; NF200: neurofilament-200; SCI: spinal cord injury; shRNA: short hairpin RNA; Tyr-tubulin: tyrosinated-tubulin.

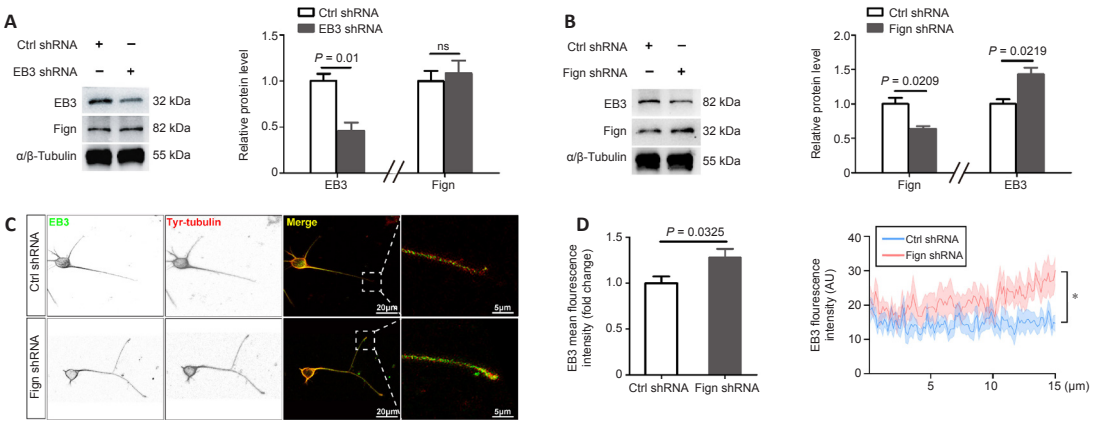

Figure 2 | **Fign knockdown increases EB3 entry into growing neurites.**
(A, B) Representative western blotting of Fign and EB3 after E18 rat cortical neurons were transfected with EB3 siRNA (A) or Fign siRNA (B) for 3 days. α/β-Tubulin was used as a loading control. The data (normalized by Ctrl siRNA group) are shown as mean ± SE (n = 3) and were analyzed by Student's t-test. (C) Representative inverted immunostaining of EB3 (green, Alexa Fluor 488) or tyrosinated (Tyr)-tubulin (red, Cy3) after E18 rat cortical neurons were transfected with Ctrl or Fign siRNA for 3 days. Increased amount of EB3 at neurite ends in the Fign siRNA group. Scale bars: 20 μm, 5 μm (enlarged images). (D) Statistical results of EB3 levels (n = 14) and fluorescence intensity (n = 10) along the last 15 μm of axons. The data (normalized by Ctrl siRNA group) are shown as mean ± SE and were analyzed by Student's t-test (left) or two-way analysis of variance followed by *post hoc* Bonferroni's test. *P < 0.05. EB3: End binding protein 3; Fign: fidgetin; siRNA: small interfering RNA; Tyr-tubulin: tyrosinated-tubulin.

distribution of these two proteins at the C-domain and P (peripheral)-domain (**Figure 3E**). Together, these results suggest that the Fign/EB3 complex is distributed along the axonal shaft and restricted to the T (transition)-zone. Thus, depletion of Fign enables greater amounts of Tyr-tubulin to break through the T-zone into the P-domain.

Fign regulates Tyr-tubulin by interacting with EB3

Next, we wanted to determine whether Fign regulates Tyr-MTs through its interaction with EB3. First, colocalization of Fign with Tyr-tubulin was verified by immunostaining (**Figure 4A**), revealing that Fign prefers to dock at Tyr-tubulin enriched MTs. Usually, tubulin newly added to the plus-end of MTs are tyrosinated. Therefore, we proposed that Fign overexpression may cause more Tyr-tubulin to move from MTs into the cytosol, resulting in more Tyr-tubulin (or free tubulin) in the supernatant. We next performed the polymerized tubulin assay, as previously described (Xu et al., 2018). Our results showed that Fign-GFP overexpression increased soluble tubulin (in the supernatant) and decreased polymerized tubulin in the pellet (**Figure 4B** and **C**). The ratio of supernatant to pellet tubulin increased to 257% after Fign overexpression. These findings suggest that Fign overexpression retained more unassembled Tyr-tubulin and free tubulin in the supernatant. In contrast, depletion of Fign notably increased Tyr-tubulin, especially at the distal end of the growing axon (**Additional Figure 2A**).

We further tested whether removal of Tyr-tubulin abolishes the function of Fign. Neurons and astrocytes were cultured and treated with Fign siRNA using the same procedure as in our previous studies (Hu et al., 2017; Ma et al., 2023). With increasing taxol (**Additional Figure 2B**), MTs became concentrated, whereas Tyr-tubulin was significantly reduced and acetylated (Ace)-tubulin increased (**Additional Figure 2C**). As expected, Fign siRNA increased Tyr-tubulin mass (**Additional Figure 2D**), whereas taxol eliminated this effect. However, when taxol was removed, Fign depletion restored the increase of Tyr-tubulin. Similarly, taxol application eliminated the increase in Tyr-tubulin in Fign siRNA-treated neurons (**Additional Figure 2E**).

To confirm the function of the interaction between Fign and EB3, we deleted EB3 by RNA interference in combination with LV5-Fign viral expression to examine the effects on Tyr-tubulin and axonal length. Fign overexpression decreased Tyr-tubulin and axonal length (**Figure 4D** and **E**), with the effects eliminated after EB3 depletion. **Figure 4F** showed increased LV5-Fign resulted in more Fign in axons. These results show that Fign trimmed Tyr-tubulin via interaction with EB3.

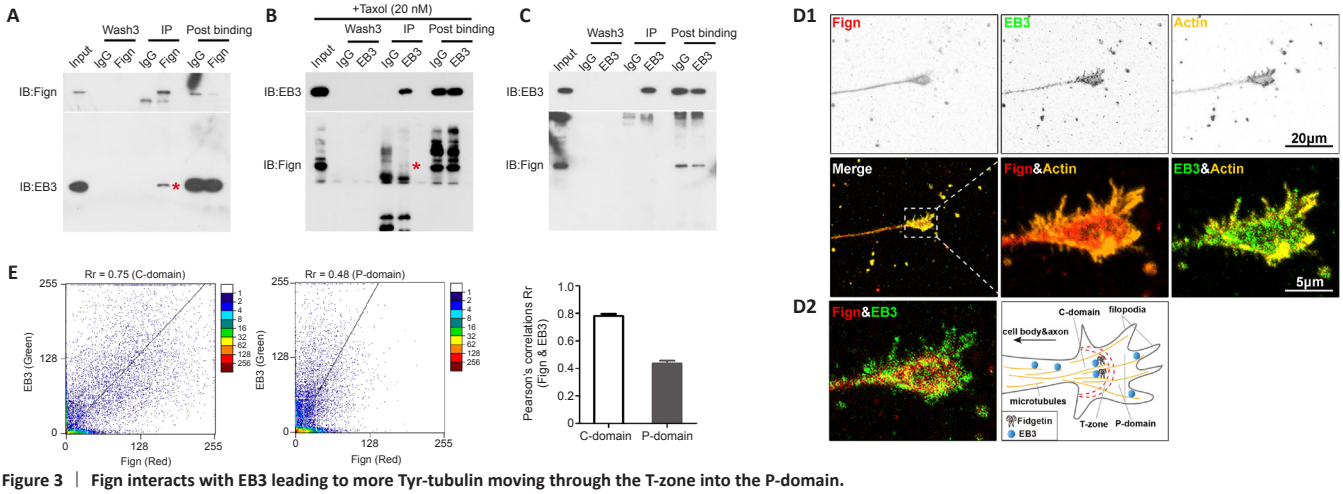

Figure 3 | **Fign interacts with EB3 leading to more Tyr-tubulin moving through the T-zone into the P-domain.**
(A) Co-immunoprecipitation between endogenous Fign and EB3. Cortical neuronal lysates from rat embryos at 18 days were immunoprecipitated with anti-Fign antibody and immunoblotted with anti-Fign (upper panel) or anti-EB3 (lower panel) antibody. (B) Lysates of neurons treated with 20 nM taxol before collection. Asterisk indicates the positive band. (C) Co-immunoprecipitation between endogenous EB3 and Fign. E18 cortical neuronal lysates were immunoprecipitated with anti-EB3 antibody and immunoblotted with anti-EB3 (upper panel) or anti-Fign (lower panel) antibody. (D1) Representative inverted immunostaining results of EB3 (green, Alexa Fluor 488), Fign (red, Alexa Fluor 647), and actin (yellow, Cy3). Scale bars: 20 μm, 5 μm (enlarged images). (D2) Enlarged immunostaining results show co-localization of EB3 and Fign. Scale bar: 5 μm. (E) Representative scatterplots of Pearson correlations for EB3 and Fign in the C-domain and P-domain (left panel). Pearson correlations of EB3 & Fign (n = 14, right panel): Rr (C-domain) = 0.78 ± 0.015 and Rr (P-domain) = 0.43 ± 0.02. EB3: End binding protein 3; Fign: fidgetin; IB: immunoblotting; IgG: non-specific antibody from same species; IP: immunoprecipitation.

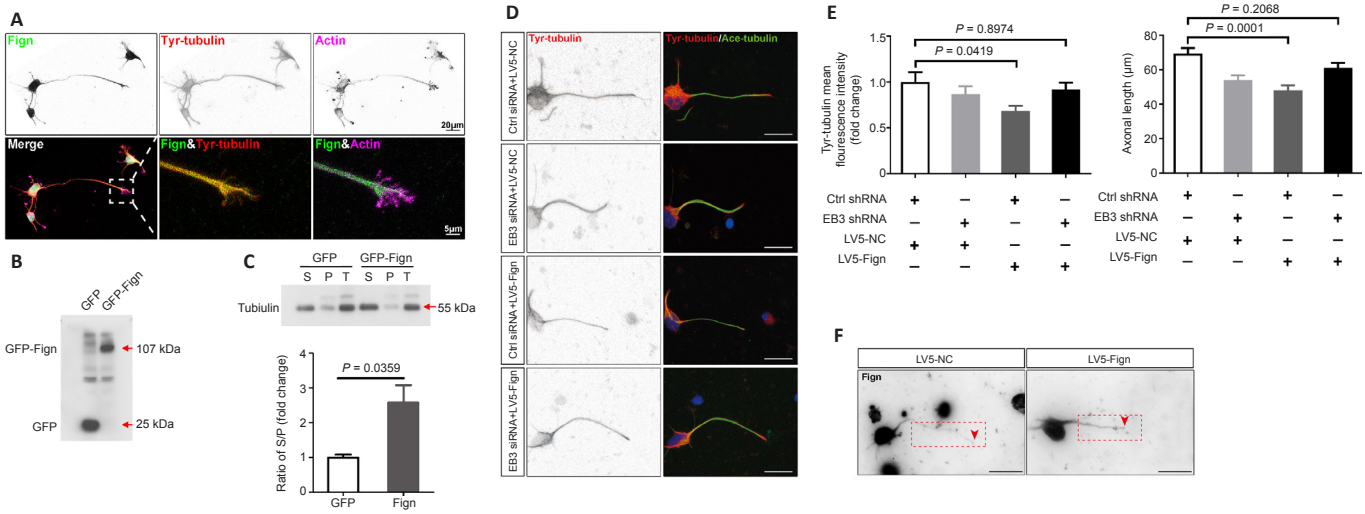

Figure 4 | **Fign regulates Tyr-tubulin by binding to EB3 and parking at microtubules plus-ends.**
(A) Representative inverted immunostaining of Fign (green, Alexa Fluor 488), tyrosinated (Tyr)-tubulin (red, Cy3), and actin (violet, Alexa Fluor 647). Scale bars: 20 μm, 5 μm (enlarged images). (B) Representative western blotting with GFP antibody after transfection of GFP or GFP-Fign plasmid to Neuro-2a cells for 2 days. (C) Representative western blotting of tubulin proteins after transfection of GFP or GFP-Fign plasmid to Neuro-2a cells for 2 days. The data (normalized by control GFP plasmid transfection) are shown as mean ± SE (n = 3), and were analyzed by Student's t-test. (D) Representative inverted immunostaining of Tyr-tubulin (red, Cy3) and acetylated-tubulin (green, Alexa Fluor 488) after E18 cortical neurons were transfected with Ctrl or EB3 siRNA and lentivirus (LV)5-NC or LV5-Fign. Ctrl siRNA combined with LV5-Fign decreased Tyr-tubulin and axonal length. EB3 siRNA combined with LV5-Fign rescued this phenomenon. Scale bar: 20 μm. (E) Statistical results of relative Tyr-tubulin levels (left panel, n = 15, normalized by Ctrl siRNA + LV5-NC group) and axonal length (right panel, n = 35) of neurons transfected with Ctrl or EB3 siRNA, together with LV5-NC or LV5-Fign. The data are shown as mean ± SE and were analyzed using one-way analysis of variance and Dunnett's test. (F) Representative inverted immunostaining of Fign in E18 cortical neurons transfected with LV5-NC or LV5-Fign. Scale bar: 20 μm. Red dotted box shows Fign in the axon. Red arrow shows the axonal terminal. Ace-tubulin: Acetylated-tubulin; E18: rat embryo at 18 days; EB3: end binding protein 3; Fign: fidgetin; GFP: green fluorescent protein; LV: lentivirus; P: pellet, tubulins in polymerized microtubules; S: supernatant, soluble tubulins; siRNA: small interfering RNA; T: total, total tubulins; Tyr-tubulin: tyrosinated-tubulin.

Discussion

It is well-known that the amount of labile domain of axonal MTs is indispensable to many axon behaviors (Konishi and Setou, 2009; Marcos et al., 2009; Nirschl et al., 2016). Post-translational modification of MTs is dynamic, turning over rapidly within the axon, and labile MTs in the axon are enriched with Tyr-tubulin (Baas and Black, 1990). Tyr-tubulin participates in organization of the cytoskeleton in growth cones and contributes to axonal branching and pathfinding (Marcos et al., 2009). Recent studies have indicated that Tyr-tubulin is a tracking signal for motor transport (Konishi and Setou, 2009; Nirschl et al., 2016).

After SCI, axonal MT tracks are destroyed and the corrupted MTs form a non-regenerative retracted bulb (Sofroniew, 2018). A clinical study reported that most patients retain residual axons (spared axons), but the injured axons cannot regenerate owing to the disordered MT lattice (Fawcett et al., 2007). Thus, increasing MT dynamics after SCI is an attractive strategy. In this study, we present a proof-of-concept investigation for testing Fign as a therapeutic target for increasing Tyr-tubulin. First, we compared differences in the amounts of Tyr-tubulin between the spinal cord and sciatic nerve in adult rats, finding more Tyr-tubulin mass in the peripheral nervous system. We further revealed that Tyr-tubulin rapidly increases, along with a sharp decrease of Fign protein, after sciatic nerve injury. This phenomenon of increased Tyr-tubulin contributes to nerve regeneration. Finally, our data suggest that augmentation of Tyr-tubulin by manipulating Fign knockdown in SCI could improve axonal regeneration and functional recovery.

A previous study has shown that Fign depletion promotes axonal growth owing to an increase in labile MTs (Leo et al., 2015), but its mechanism has been poorly studied. In this study, we reveal a molecular mechanism for the preference of Fign for Tyr-tubulin: specifically, Fign binds to the plus-end of MTs, which prunes Tyr-tubulin via interaction with EB3. EB3 proteins are abundant in neurons. They bind to the growing tips of MTs and recruit essential factors to modulate MT dynamics. A report stated that EB3 binding zones on MTs frequently exhibit stationary EB3 islands. This suggests that unknown proteins could form a complex with EB3, thereby prolonging residence time on MTs, or simultaneously bind with tubulin and EB3, thereby increasing EB3 affinity for MTs (Mustyatsa et al., 2019). Similar reports indicated that interaction of EB3 and inositol-trisphosphate 3-kinase A facilitated MT remodeling in synapses in response to stimulation; additionally, the combination of EB3 and kinesin-13 promoted a fast switch between MT polymerization and depolymerization (Montenegro Gouveia et al., 2010; Mo et al., 2019), thus rearranging the MT cytoskeleton. Therefore, our study shows EB3 carries Fign on MTs to provide a platform for Fign function. When Fign was knocked-down, more Tyr-tubulin was retained at MT plus-ends, and more EB3 molecules entered MT plus-ends and promoted MT assembly, thereby increasing axonal length.

This study has limitations: one is that female rats were excluded from our *in vivo* study to avoid the effects of estrogen, and also because there are more male patients in the clinic with SCI than female patients. Another limitation relates to whether other molecules exist in the Fign/EB3 complex, which should be further studied. In summary, our study reports for the first time that Fign interacts with EB3 to dock at the growing end of MTs. The mechanism of Fign action suggests that EB3 carries Fign to the MT plus-ends during axonal growth, which enriches new Tyr-tubulin. Fign works as a sever to prune MT plus-ends and contributes to correct pathfinding and proper branching. Therefore, addition of Tyr-tubulin extends the labile end of MTs, thus facilitating axon regeneration after Fign removal.

In conclusion, this study suggested that Fign knockdown is beneficial to the recovery of spinal cord injury and might be a potential therapeutic target.

Author contributions: *Study design and management, and manuscript production: CM, LQ, and ML; experimental implementation: CM, JW, QT, WB, ZH, RZ and RW; data analysis: CM, ZD, LQ, YL, and ML. All authors have read and approved the final version of the manuscript.*
Conflicts of interest: *The authors declare no competing interests in this work.*
Data availability statement: *All data relevant to the study are included in the article or uploaded as Additional files.*

Editor's evaluation: *A very interesting and important story has been emerging on the importance of labile microtubule domains in axon regeneration. The authors take the story a significant step forward in three ways. First, they document a physiological fidgetin response in peripheral nerves that do regeneration compared to spinal cord nerves that do not. Second, they show that the therapeutic knockdown of fidgetin in the spinal cord results in functional recovery and axon regeneration. Third, they show that fidgetin is associated with EB3 in a manner that can explain, mechanistically, how fidgetin targets the labile domains of the microtubules.*
Additional files:
Additional Figure 1: *Depletion of Fign increases the axonal length and branches.*
Additional Figure 2: *Depletion of Fign increases the Tyr-tubulins.*

References

Ahmad FJ, Yu W, McNally FJ, Baas PW (1999) An essential role for katanin in severing microtubules in the neuron. J Cell Biol 145:305-315.
Anderson MA, O'Shea TM, Burda JE, Ao Y, Barlatey SL, Bernstein AM, Kim JH, James ND, Rogers A, Kato B, Wollenberg AL, Kawaguchi R, Coppola G, Wang C, Deming TJ, He Z, Courtine G, Sofroniew MV (2018) Required growth facilitators propel axon regeneration across complete spinal cord injury. Nature 561:396-400.
Austin TO, Matamoros AJ, Friedman JM, Friedman AJ, Nacharaju P, Yu W, Sharp DJ, Baas PW (2017) Nanoparticle delivery of fidgetin siRNA as a microtubule-based therapy to augment nerve regeneration. Sci Rep 7:9675.
Baas PW, Black MM (1990) Individual microtubules in the axon consist of domains that differ in both composition and stability. J Cell Biol 111:495-509.
Basso DM, Beattie MS, Bresnahan JC (1995) A sensitive and reliable locomotor rating scale for open field testing in rats. J Neurotrauma 12:1-21.
Blanquie O, Bradke F (2018) Cytoskeleton dynamics in axon regeneration. Curr Opin Neurobiol 51:60-69.
Cao XM, Li SL, Cao YQ, Lv YH, Wang YX, Yu B, Yao C (2022) A comparative analysis of differentially expressed genes in rostral and caudal regions after spinal cord injury in rats. Neural Regen Res 17:2267-2271.
Cho Y, Cavalli V (2012) HDAC5 is a novel injury-regulated tubulin deacetylase controlling axon regeneration. EMBO J 31:3063-3078.
Cox GA, Mahaffey CL, Nystuen A, Letts VA, Frankel WN (2000) The mouse fidgetin gene defines a new role for AAA family proteins in mammalian development. Nat Genet 26:198-202.
Fawcett JW, Curt A, Steeves JD, Coleman WP, Tuszynski MH, Lammertse D, Bartlett PF, Blight AR, Dietz V, Ditunno J, Dobkin BH, Havton LA, Ellaway PH, Fehlings MG, Privat A, Grossman R, Guest JD, Kleitman N, Nakamura M, Gaviria M, et al. (2007) Guidelines for the conduct of clinical trials for spinal cord injury as developed by the ICCP panel: spontaneous recovery after spinal cord injury and statistical power needed for therapeutic clinical trials. Spinal Cord 45:190-205.
Feng J, Hu Z, Chen H, Hua J, Wu R, Dong Z, Qiang L, Liu Y, Baas PW, Liu M (2016) Depletion of kinesin-12, a myosin-IIB-interacting protein, promotes migration of cortical astrocytes. J Cell Sci 129:2438-2447.
Fukushima N, Furuta D, Hidaka Y, Moriyama R, Tsujiuchi T (2009) Post-translational modifications of tubulin in the nervous system. J Neurochem 109:683-693.
Hu Z, Feng J, Bo W, Wu R, Dong Z, Liu Y, Qiang L, Liu M (2017) Fidgetin regulates cultured astrocyte migration by severing tyrosinated microtubules at the leading edge. Mol Biol Cell 28:545-553.
Hur EM, Saijilafu, Zhou FQ (2012) Growing the growth cone: remodeling the cytoskeleton to promote axon regeneration. Trends Neurosci 35:164-174.
Ji Z, Zhang G, Chen L, Li J, Yang Y, Cha C, Zhang J, Lin H, Guo G (2018) Spastin interacts with CRMP5 to promote neurite outgrowth by controlling the microtubule dynamics. Dev Neurobiol 78:1191-1205.
Konishi Y, Setou M (2009) Tubulin tyrosination navigates the kinesin-1 motor domain to axons. Nat Neurosci 12:559-567.
Kulkarni R, Thakur A, Kumar H (2022) Microtubule dynamics following central and peripheral nervous system axotomy. ACS Chem Neurosci 13:1358-1369.
Lasiene J, Shupe L, Perlmutter S, Horner P (2008) No evidence for chronic demyelination in spared axons after spinal cord injury in a mouse. J Neurosci 28:3887-3896.
Leo L, Yu W, D'Rozario M, Waddell EA, Marenda DR, Baird MA, Davidson MW, Zhou B, Wu B, Baker L, Sharp DJ, Baas PW (2015) Vertebrate fidgetin restrains axonal growth by severing labile domains of microtubules. Cell Rep 12:1723-1730.
Liu J, Li L, Zou Y, Fu L, Ma X, Zhang H, Xu Y, Xu J, Zhang J, Li M, Hu X, Li Z, Wang X, Sun H, Zheng H, Zhu L, Guo J (2022) Role of microtubule dynamics in Wallerian degeneration and nerve regeneration after peripheral nerve injury. Neural Regen Res 17:673-681.
Ma C, Teng L, Lin G, Guo B, Zhuo R, Qian X, Guan T, Wu R, Liu Y, Liu M (2021) L-leucine promotes axonal outgrowth and regeneration via mTOR activation. FASEB J 35:e21526.
Ma C, Wang J, Tu Q, Wu R, Lai X, Lin G, Dong Z, Guan T, Qiang L, Liu Y, Liu M (2023) Fidgetin impacts axonal growth and branching in a local mTOR signal dependent manner. Exp Neurol 361:114315.
Marcos S, Moreau J, Backer S, Job D, Andrieux A, Bloch-Gallego E (2009) Tubulin tyrosination is required for the proper organization and pathfinding of the growth cone. PLoS One 4:e5405.
Matamoros AJ, Tom VJ, Wu D, Rao Y, Sharp DJ, Baas PW (2019) Knockdown of fidgetin improves regeneration of injured axons by a microtubule-based mechanism. J Neurosci 39:2011-2024.
McNally FJ, Roll-Mecak A (2018) Microtubule-severing enzymes: from cellular functions to molecular mechanism. J Cell Biol 217:4057-4069.
Min ZY, Aali M, Zheng YH, Zeng XZ, Bian NY, Deng SS, Xie J (2022) Mechanism and characteristics of mechanical microenvironment of extracellular matrix and intercellular interaction. Zhongguo Zuzhi Gongcheng Yanjiu 26:4034-4045.
Mo SJ, Cho Y, Choi BI, Lee D, Kim H (2019) PKA-dependent phosphorylation of IP3K-A at Ser119 regulates a binding affinity with EB3. Biochem Biophys Res Commun 508:52-59.
Montenegro Gouveia S, Leslie K, Kapitein LC, Buey RM, Grigoriev I, Wagenbach M, Smal I, Meijering E, Hoogenraad CC, Wordeman L, Steinmetz MO, Akhmanova A (2010) In vitro reconstitution of the functional interplay between MCAK and EB3 at microtubule plus ends. Curr Biol 20:1717-1722.
Mukherjee S, Diaz Valencia JD, Stewman S, Metz J, Monnier S, Rath U, Asenjo AB, Charafeddine RA, Sosa HJ, Ross JL, Ma A, Sharp DJ (2012) Human Fidgetin is a microtubule severing the enzyme and minus-end depolymerase that regulates mitosis. Cell Cycle 11:2359-2366.
Mustyatsa VV, Kostarev AV, Tvorogova AV, Ataullakhanov FI, Gudimchuk NB, Vorobjev IA (2019) Fine structure and dynamics of EB3 binding zones on microtubules in fibroblast cells. Mol Biol Cell 30:2105-2114.
Nirschl JJ, Magiera MM, Lazarus JE, Janke C, Holzbaur EL (2016) α-Tubulin tyrosination and CLIP-170 phosphorylation regulate the initiation of dynein-driven transport in neurons. Cell Rep 14:2637-2652.
Qiang L, Sun X, Austin TO, Muralidharan H, Jean DC, Liu M, Yu W, Baas PW (2018) Tau does not stabilize axonal microtubules but rather enables them to have long labile domains. Curr Biol 28:2181-2189.e4.
Qu X, Kumar A, Blockus H, Waites C, Bartolini F (2019) Activity-dependent nucleation of dynamic microtubules at presynaptic boutons controls neurotransmission. Curr Biol 29:4231-4240.e5.
Roll-Mecak A, McNally FJ (2010) Microtubule-severing enzymes. Curr Opin Cell Biol 22:96-103.
Schneider CA, Rasband WS, Eliceiri KW (2012) NIH image to ImageJ: 25 years of image analysis. Nat Methods 9:671-675.
Shin SC, Im SK, Jang EH, Jin KS, Hur EM, Kim EE (2019) Structural and molecular basis for katanin-mediated severing of glutamylated microtubules. Cell Rep 26:1357-1367.e5.
Sofroniew MV (2018) Dissecting spinal cord regeneration. Nature 557:343-350.
Song Y, Brady ST (2015) Post-translational modifications of tubulin: pathways to functional diversity of microtubules. Trends Cell Biol 25:125-136.
Tao J, Feng C, Rolls MM (2016) The microtubule-severing protein fidgetin acts after dendrite injury to promote their degeneration. J Cell Sci 129:3274-3281.
Teng L, Guan T, Guo B, Ma C, Lin G, Wu R, Xu M, Liu M, Liu Y (2021) GIP-GIPR promotes neurite outgrowth of cortical neurons in Akt dependent manner. Biochem Biophys Res Commun 534:121-127.
Vemu A, Szczesna E, Zehr EA, Spector JO, Grigorieff N, Deaconescu AM, Roll-Mecak A (2018) Severing enzymes amplify microtubule arrays through lattice GTP-tubulin incorporation. Science 361:eaau1504.
Witte H, Neukirchen D, Bradke F (2008) Microtubule stabilization specifies initial neuronal polarization. J Cell Biol 180:619-632.
Wu R, Yan Y, Yao J, Liu Y, Zhao J, Liu M (2015) Calpain 3 expression pattern during gastrocnemius muscle atrophy and regeneration following sciatic nerve injury in rats. Int J Mol Sci 16:26927-26935.
Wu R, Mao S, Wang Y, Zhou S, Liu Y, Liu M, Gu X, Yu B (2019) Differential circular RNA expression profiles following spinal cord injury in rats: a temporal and experimental analysis. Front Neurosci 13:1303.
Xu GJ, Zhang Q, Li SY, Zhu YT, Yu KW, Wang CJ, Xie HY, Wu Y (2021) Environmental enrichment combined with fasudil treatment inhibits neuronal death in the hippocampal CA1 region and ameliorates memory deficits. Neural Regen Res 16:1460-1466.
Xu X, Wicki-Stordeur LE, Sanchez-Arias JC, Liu M, Weaver MS, Choi CSW, Swayne LA (2018) Probenecid disrupts a novel pannexin 1-collapsin response mediator protein 2 interaction and increases microtubule stability. Front Cell Neurosci 12:124.
Yu W, Qiang L, Solowska JM, Karabay A, Korulu S, Baas PW (2008) The microtubule-severing proteins spastin and katanin participate differently in the formation of axonal branches. Mol Biol Cell 19:1485-1498.
Zhao PF, Yu RH, Hua J, Wang P, Liu M (2017) Effect of Kinesin-12 knockdown on morphology and function after rat spinal cord injury. Nantong Daxue Xuebao: Yixue Ban 37:1-5.

C-Editor: Zhao M; S-Editors: Yu J, Li CH; L-Editors: Yu J, Song LP; T-Editor: Jia Y

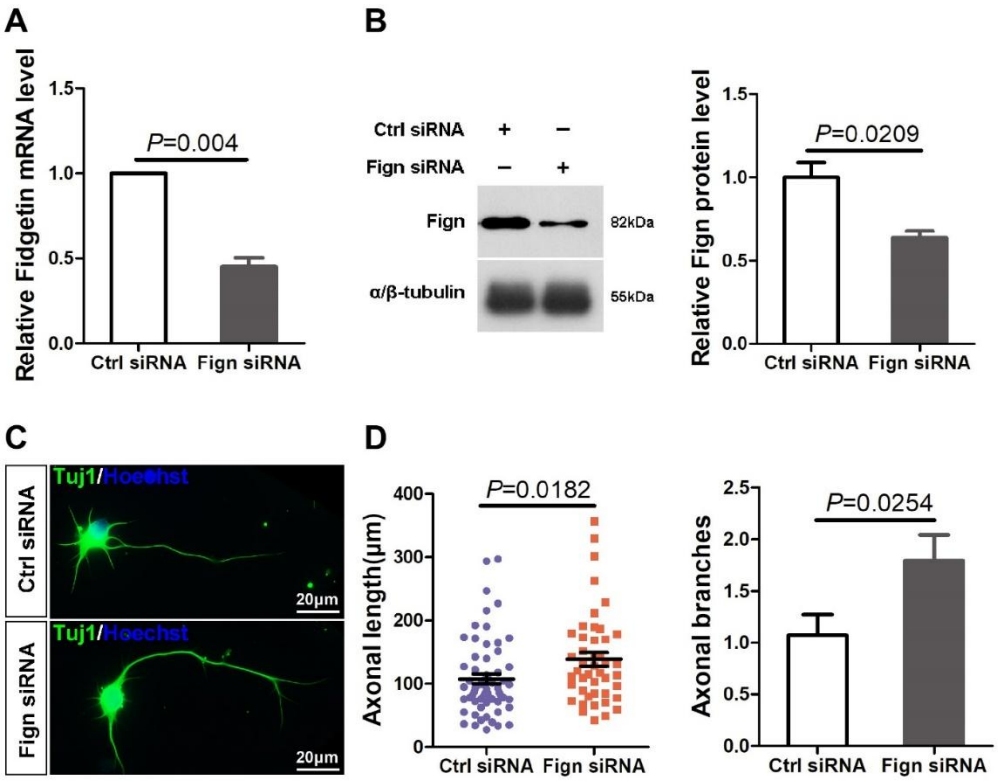

Additional Figure 1 Depletion of Fign increases the axonal length and branches.

(A) Representative quantitative polymerase chain reaction results of Fign after E18 rat cortical neurons transfected with Ctrl or Fign siRNA for 3 days. The data were normalized by Ctrl siRNA group (n = 3). (B) Representative western blotting of Fign after E18 rat cortical neurons transfected with Ctrl or Fign siRNA for 3 days. α/β-Tubulin was used as a loading control. The data were normalized by Ctrl siRNA group (n = 3). (C) Representative immunostaining results of Tuj1 (green, Alexa Fluor 488) after E18 rat cortical neurons transfected with Ctrl or Fign siRNA for 3 days. Fign siRNA group increased axonal length and number of branches. Scale bars: 20 μm. (D) Statistical result of axonal length (n = 45) and axonal branches (n = 48) of neurons transfected with Ctrl or Fign siRNA by immunofluorescence. All data in A, B, and D are shown as mean ± SE, and were analyzed by Student's t-test. E18: Rat embryo at 18 days; Fign: fidgetin; siRNA: small interfering RNA.

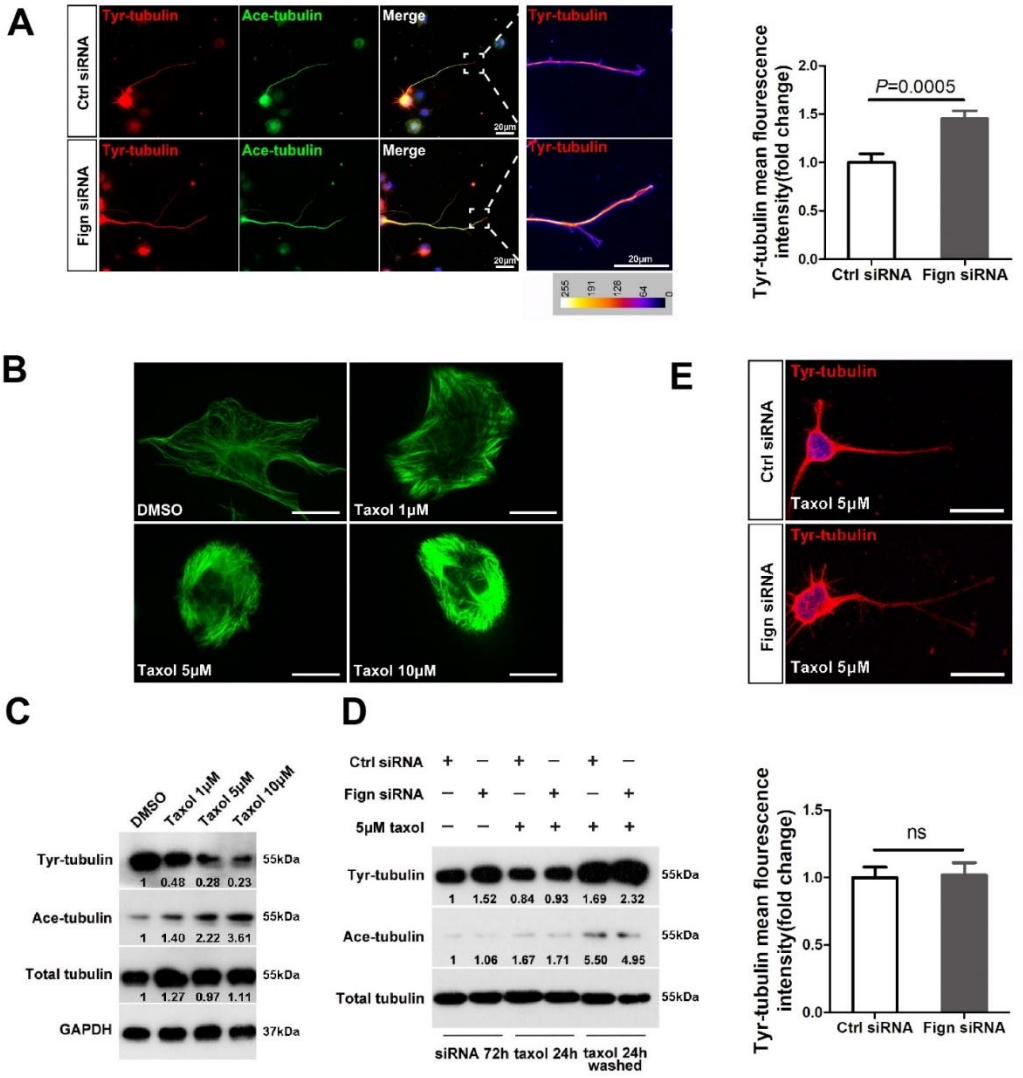

Additional Figure 2 Depletion of Fign increases the Tyr-tubulins.

(A) Representative immunostaining results of Tyr-tubulin (red, Cy3) or Ace-tubulin (green, Alexa Fluor 488) after E18 rat cortical neurons transfected with Ctrl or Fign siRNA. Scale bars: 20 μm. Quantitative results were normalized by Ctrl siRNA group (n = 21). (B, C) Representative immunostaining images (B) of α-tubulin (green, Alexa Fluor 488), and western blotting result (C) of Tyr-tubulin and Ace-tubulin after astrocytes treated with DMSO, or Taxol (1, 5, 10 μM). Microtubules in astrocytes become more polymerized after adding taxol. Scale bar: 20 μm. GAPDH was used as a loading control. (D) Representative western blotting results of Tyr-tubulin and Ace-tubulin in astrocytes transfected with Ctrl or Fign siRNA with or without taxol, or taxol washed out. Total tubulin was used as a loading control. (E) Representative immunostaining results of Tyr-tubulin (red, Cy3) in E18 rat cortical neurons transfected with Ctrl or Fign siRNA treated with Taxol (5 μM). There was no significant difference in Tyr-tubulin expression (normalized by Ctrl siRNA group) between the two groups after adding taxol (n = 11). Scale bar: 20 μm. All data in A and E are shown as mean ± SE, and were analyzed by Student's *t*-test. Ace-tubulin: Acetylated-tubulin; DMSO: dimethyl sulfoxide; Fign: fidgetin; GAPDH: glyceraldehyde-3-phosphate dehydrogenase; siRNA: small interfering RNA; Tyr-tubulin: tyrosinated-tubulin.